Research Article

# Role of gelatin and chitosan cross-linked aqueous template in controlling the size of lithium titanium oxide

Parbhej Ahamed[1] · William Ghann[2] · Jamal Uddin[2] · Mohammad A. Yousuf[1]

Received: 30 July 2021 / Accepted: 14 November 2021
Published online: 22 March 2022


**Abstract**
Significant safety advantages of lithium titanium oxide (LTO) over currently used graphite for lithium-ion batteries have been attracting scientists to develop novel synthetic methods of this anode material in order to combine with another cathode. This study utilizes self-sacrificing cross-linked aqueous templates of gelatin and chitosan polymer to control lithium titanium oxide (LTO) morphology and microstructure. Gelatin and chitosan self-assembled aqueous template containing LTO precursors has been evaporated at 110 °C and then calcined at 750 °C in a muffle furnace to synthesize white color LTO powder. Various techniques such as X-ray diffraction (XRD), field emission scanning electron microscopy (FESEM), Energy dispersive x-ray spectroscopy (EDS), Fourier transform infrared spectroscopy (FT-IR), Raman spectroscopy and UV–visible spectroscopy were used to characterize the synthesized LTO powders. Both XRD and EDS spectrum confirm the coating of gelatin and chitosan derived carbon species on the surface of LTO materials. The detailed characterization reveals that increasing the amount of gelatin to the mass ratio of gelatin and chitosan reduced LTO particle sizes. Thus, a size controlled carbon coating LTO preparation strategy have been established via gelatin and chitosan cross-linked aqueous template in controlling the morphology and microstructure of LTO material.

**Keywords** Self-sacrificing polymer template · Gelatin · Chitosan · Lithium titanium oxide · Li-ion battery

## 1 Introduction

Soft chemistry routes such as sol–gel [1], long-chain polymers [2], surfactants [3], organic molecules [4], structure directing agents [5] and biologic species [6] have been considered as an effective method for preparing composite material oxides. These soft materials serve template of fixed sizes and morphologies to mix precursor metal ions uniformly at atomic or molecular levels. Interactions between metal ions and soft material functional groups confined the raw materials in the template. Composite materials structure, shape, size, properties and functions scale with confinement geometry of metal ions into soft material templates. Moreover, a soft templates process is a widely used environment friendly, non-toxic route of preparing porous composite materials. This technique plays a key role for the preparation of innovative materials in fields such as inorganic chemistry [7], materials science [8], organic chemistry [9] and bio-technology [10] for searching their potential applications in electrode materials [11], super-capacitors [12], solar cells [13] and photo-catalysts [14]. It becomes a useful means to link the design and application of composite materials for enabling their full potentiality in the aforementioned fields. The convenient template to design and prepare the composite materials in the area of soft chemistry routes are still developing to

✉ Mohammad A. Yousuf, yousuf@chem.kuet.ac.bd | [1]Department of Chemistry, Khulna University of Engineering and Technology, Khulna 9203, Bangladesh. [2]Center for Nanotechnology, Department of Natural Sciences, Coppin State University, Baltimore, MD 21216, USA.

meet the needs of the materials for further improvement in their respective application area.

Accordingly, few attempts such as phenol–formaldehyde resin [15], poly-styrene-b-poly(4-vinylpyridine) [16], gelatin [17, 18], polyethylene glycol [19], alginic acid [11] self-sacrificing polymer templating have been made to prepare $Li_4Ti_5O_{12}$, $LiCoO_2$/$Li_7La_3Zr_2O_{12}$, $Co_3O_4$ for using as electrode materials in lithium ion batteries (LIBs). Among the synthesized electrode material spinel lithium titanium oxide ($Li_4Ti_5O_{12}$/LTO) has been suggested as a promising new generation potential anode material for large scale implementation of LIB [20]. It has been regarded as a zero strain and low cost material with excellent cyclic stability at operating voltage of 1.55 V vs. $Li^+$/Li [21–24]. It exhibited negligible volume changes during Li + ions intercalation and extraction processes. The material possessed long cycle life, good rate performance, excellent safety performance and high prospect to replace the present graphite based commercial anode material of LIBs [25, 26]. The commercial electrode fabrication processes of LTO have been hindered from its morphology and microstructure aspect of low electronic conductivity. To overcome the commercialization shortcomings of LTO the aforementioned self-sacrificing polymer templating have been prepared LTO electrode materials with controlled particle size, even homogeneity and ordered structure over the common heteroatom doping [27–29] and surface modification [30–33] methods of LTO material. Furthermore, the electrode materials were prepared without the need of special equipment, expensive reagents and complexity. It is also found that the prepared electrode material properties improved significantly with these polymer templating methods. However, the method still needs more development direction to prepare right morphologies and microstructures LTO for next generation LIBs.

Concerning the aforementioned progress cross-linking of two macromolecules may become an interesting approach in the preparation of homogeneous and uniform size LTO material on substitution of single polymer matrix. Attention has been thereby paid for controlling LTO particle sizes through the polymer engineering of gelatin and chitosan. We anticipate that the size and morphology of LTO particles can be controlled by the amount of the aforementioned polymer matrices. Hence, we employed environmentally friendly gelatin [34] and chitosan [35] polymer cross-linked aqueous template for the preparation of LTO material. The cross-linked polymers network has been identified as a simple and effective method for controlling LTO sizes with the amount of polymers. Finally, we have been provide the role of gelatin-chitosan cross-linked aqua framework by means of polymers amount to compute LTO sizes.

## 2 Experimental

### 2.1 Materials and reagents

All the chemicals were used as received. The details of the used materials are given in the following Table 1.

### 2.2 Preparation of lithium titanium oxide (LTO) powder

LTO materials were synthesized from gelatin and chitosan mass ratio of 1:2, 1:1, 3:2 and 2:1 which were identified as GC1, GC2, GC3 and GC4, respectively. Chitosan was taken in a beaker. 20 mL deionized water and 0.5 mL 0.01 M acetic acid solutions were added to it. It was stirred 30 min at room temperature. Gelatin was then added to this solution to maintain a certain chitosan: gelatin weight ratio. The exact amount of gelatin and chitosan for maintaining different weight ratio are listed in the following Table 2.

The mixture was stirred at 50 °C for 30 min. The solution turned to viscous upon cooled down to room temperature. Stoichiometric amount of 1.1831 g lithium hydroxide and 2.8168 g titanium (IV) oxide were dispersed to the viscous solution and stirred 24 h at room

**Table 1** List of used materials

| Name of chemicals | Formula | Name of company | Properties |
|---|---|---|---|
| Lithium hydroxide (Monohydrate) | $LiOH.H_2O$ | Loba Chemie Co. Ltd, India | Purity ≥ 98.50% |
| Titanium (IV) oxide | $TiO_2$ | Merck chemical company, India | Purity ≥ 99.5%<br>Crystal = Rutile |
| Chitosan | $(C_6H_{11}NO_4)_n$ | Sisco Research Laboratories Pvt. Ltd, India | Molecular weight ~ 193,400 |
| Gelatin | $(C_{102}H_{151}N_{31}O_{39})_n$ | Opsonin Pharma, Bangladesh | Purity ≥ 98%<br>Molecular weight ~ 1,00,000–200,000 |
| Acetic acid | $CH_3COOH$ | Merck chemical company, India | Purity ≥ 99<br>pH = 5 |
| Milopore water | $H_2O$ | From laboratory | Purity ≥ 99 |

**Table 2** Amount of gelatin and chitosan for maintaining different weight ratio

| Sample | Weight ratio | Gelatin (g) | Chitosan (g) |
|---|---|---|---|
| GC1 | 1: 2 | 0.03 | 0.07 |
| GC2 | 1: 1 | 0.05 | 0.05 |
| GC3 | 3: 2 | 0.06 | 0.04 |
| GC4 | 2: 1 | 0.07 | 0.03 |

temperature to organize the precursor materials in the cross-linked framework. After stirring, the solution was heated at 110 °C for 2 h for the removal of solvent. Finally, calcination of the residue at 750 °C for 6 h in a muffle furnace in presence of oxygen yielded white color LTO powder.

## 2.3 Characterization

### 2.3.1 Powder x-ray diffraction (XRD)

Powder X-ray diffraction data of the prepared LTO samples were collected using Bruker Advance D8 XRD diffractometer equipped with $CuK_{\alpha}$ monochromated beam ($\lambda = 0.15406$ Å). Accelerating voltage 40 kV, accelerating current 40 mA, scan step 0.02 degrees and scan rate 0.01 s/step were other test conditions for 0° to 90° scan range. A small amount of the prepared LTO powder was poured into the sample holders of the diffractometer. After loading the sample holder was mounted on the diffractometer and scanned. The interplanar spacing of the prepared LTO samples has been calculated using the following Bragg's equations [36].

$$2d \sin\theta = n\lambda \quad (1)$$

where $n$ is the order of diffraction (usually $n = 1$), λ is the X-ray wavelength and d is the spacing between planes of given Miller indices h, k and l.

### 2.3.2 Field emission scanning electron microscopy (FESEM)

Morphological changes of the synthesized LTO samples were investigated using field emission scanning electron microscopy technique. Few drops of LTO suspended in ethanol solution were added on conductive carbon tape adhered to alumina plate. A sufficient period of time was then waited to dry the solution on the carbon tape. The surface of the tape was blown with air blower to remove excess powder from the sample plate. After that FESEM imaging was done using 15.0 kV operating voltage.

**Table 3** Viscosity values for different aqueous solution of gelatin and chitosan

| Solution | Viscosity (mPa.s) |
|---|---|
| GC1 | 1.3619 |
| GC2 | 1.3630 |
| GC3 | 1.3642 |
| GC4 | 1.3647 |

### 2.3.3 Raman spectroscopy

Raman Studies of the samples were performed using a model DXR smart Raman spectrometer (Thermo Fisher Scientific Co., Ltd., USA). The measurement was carried with a excitation wavelength of 780 nm full range grating.

### 2.3.4 Fourier transform infrared spectroscopy (FT-IR)

A small amount (about 1%) of the prepared LTO materials was well mixed with KBr to prepare sample for FT-IR measurements. A manual hydraulic press machine was used to make a transparent pellet from the LTO and KBr mixture. The spectrum of the prepared pellet was recorded at 16 $cm^{-1}$ resolution in the wave number range from 500 to 4000 $cm^{-1}$ using FT-IR Tracer-100 of Shimadzu Corporation, Japan.

### 2.3.5 UV–visible spectroscopy

0.01 g LTO suspended in 30 mL ethanol solution was taken in a cuvette. The cuvette was put into its holder to measure UV–visible spectrum of the respective sample. The spectrum was recorded in the range 200—800 nm using a UV-1800 spectrophotometer of Shimadzu Corporation, Japan. Tauc plot is used to calculate the band gap energy of the LTO samples on the basis of following formula [37].

$$(\alpha h\nu)^{1/n} = A\left(E - E_g\right) \quad (2)$$

where α is the absorption coefficient, A is a constant, $E = h\nu$ is the photon energy, $E_g$ is the band gap energy, and $n = 1/2$ for direct transition of electron.

# 3 Results and discussion

Gelatin as well as chitosan have good dispersion ability in water. Both have been well dispersed in water. The viscosity of the solution have been measured at 25 °C using Ostwald viscometer and listed in Table 3.

Variation of viscosity values have been resulted due to the different weight ratio of gelatin and chitosan in water. Their electrostatic interaction in water formed

interpenetrating self-assemble soft aqueous template through the formation of amide bond [38]. These soft templates were filled up with the dispersion of LTO precursors $TiO_2$ and LiOH. $TiO_2$ is inert to the amide bond. At room temperature LiOH is not quite effective to break the amide linkage. Hence, the LTO precursor's filled gelatin-chitosan cross-linked template was evaporated to remove solvent and its subsequent calcination yielded LTO sample. The prepared LTO samples were characterized by using XRD, FESEM, FT-IR and UV–visible spectroscopy techniques. The obtained results were discussed to show a relationship of gelatin and chitosan mass ratio on the prepared LTO samples. The synthetic pathway of LTO samples is shown in Fig. 1.

The Reitveld refinement XRD patterns of the four LTO samples are shown in Fig. 2. The obtained XRD patterns of LTO samples are assigned in accordance with JCPDS card No. 00–049-0207. Peaks assigned at various 2θ positions of (111), (220), (311), (400), (331), (333), (440) and (531) planes are suggesting the crystalline planes of Fd3m space groups in the structure of prepared LTO materials [39]. All of the observed diffraction peaks have been indicated the formation of pure and highly crystalline LTO materials. The peaks of reduced graphene oxide and graphite appear at 25° and 27° respectively [40]. The carbon species could have been generated from the calcination reaction of gelatin and chitosan template. They have not been changed the prepared LTO crystal structure. Hence, carbon on the surface of LTO. Very weak peaks of those carbon species are observed in the XRD pattern of GC1 sample. However, the intensity of the peaks becomes sharper and stronger with increasing gelatin amount to the mass ratio of gelatin and chitosan mixture. It has been reported that the specific capacity, conductivity, and cyclic performance of carbon coated LTO significantly improved with carbon coating. Gelatin and chitosan derived carbon might have been improved the mentioned electrical properties of LTO. Here, we could not examine those carbon related properties of LTO due to instrument limitations.

The exact crystalline phases of the prepared LTO samples have been analyzed using Reitveld refinement method. The FULLPROF software was adopted for Reitveld refinement analyses. Figure 3 shows the refined XRD profiles of the LTO samples. The refined XRD profiles also indicate that the prepared samples LTO exhibit single phase crystallinity with a trace amount of carbon species. The well-fitting of $Y_{obs}$ and $Y_{calc}$ peak shapes illustrated the presence of single crystal LTO electrode materials.

The interplanar spacing d for cubic crystal structure of LTO is related to the lattice constants by the following equation [36]. It is used to calculate lattice constant "a".

$$\frac{1}{d_{hkl}^2} = \frac{h^2 + k^2 + l^2}{a^2} \tag{3}$$

The position of the X-ray peaks, interplanar spacing, corresponding miller indices and calculated lattice constant

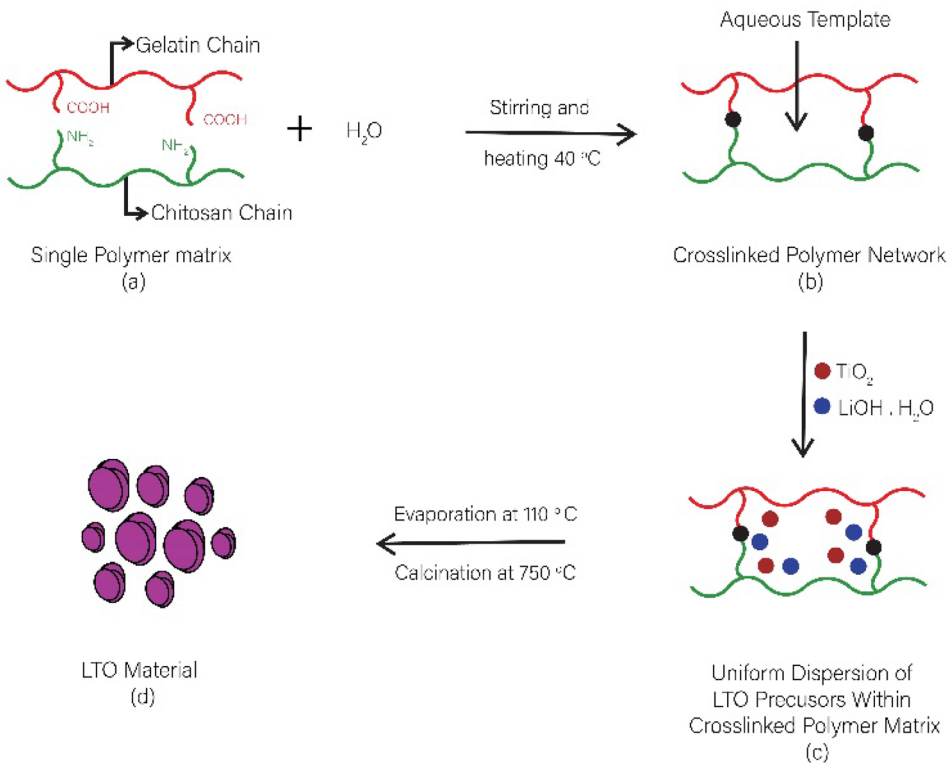


**Fig. 1** Schematic diagram for the preparation of LTO

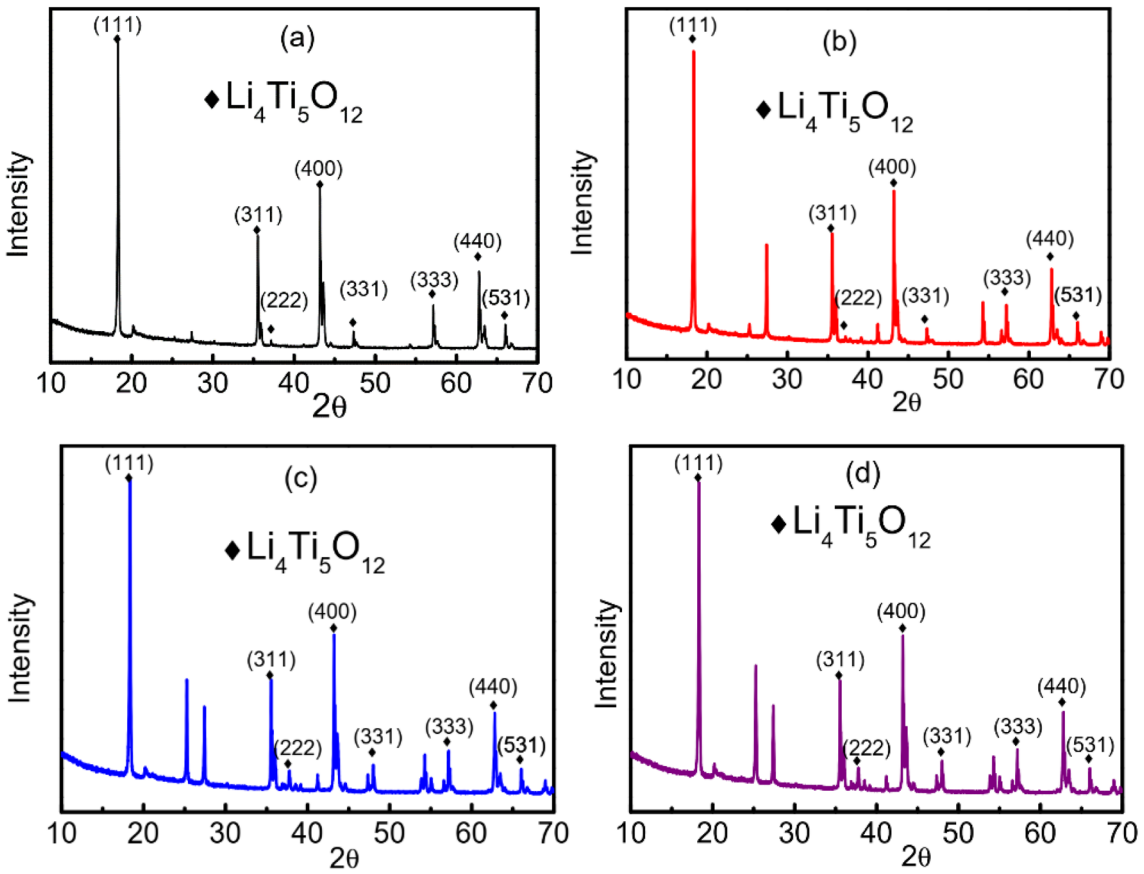


**Fig. 2** XRD spectrum of the prepared LTO material of **a** GC1 **b** GC2 **c** GC3 **d** GC4 samples

of the prepared LTO samples are summarized in Table 4. Average lattice constant value is then used for calculating unit cell volume ($V = a^3$) of the prepared LTO sample. It is worth nothing that the (111) peak of the prepared LTO shifts to higher angle with increasing the amount of gelatin in the mass ratio of gelatin and chitosan. It may be the effect of higher intermolecular interaction of gelatin and chitosan on the size of aqueous template, and hence the shift of (111) peak as a result of the reduction of the LTO particles size. The crystallite size of the prepared LTO samples for each diffraction plane was calculated by using Scherer's equation ($D = 0.9\lambda/\beta \cos\theta$) and then averaged. The calculated sizes are 94, 75, 69 and 64 nm for GC1, GC2, GC3 and GC4 samples, respectively. So, amount of carbon sources has influence on the average size of LTO. More amount of carbon sources have been suppressed particle growth during calcination and produced smaller size of LTO. Thus, it can be inferred that the amount of gelatin and chitosan plays an important role to tune the crystallite sizes of LTO powders.

The cross-linking reaction of gelatin chains with chitosan chains have been resulted the formation of micro size pore. Raw materials aggregated in between the chains of gelatin and chitosan. Pores occupied by the raw materials acts as a reaction channel during the combustion reaction for the formation of LTO particles. Size of this pore depends on the degree cross-linking between gelatin and chitosan. Here, we varied the amount of gelatin by keeping the amount of chitosan constant to assess the effect of cross-linking on the lattice constant of spinel LTO. We have found that the lattice constant value of LTO decreased with increasing the amount of gelatin. This is resulted due to the high degree of cross-linking of gelatin and chitosan. Field emission scanning electron microscopy linked to energy dispersive X-ray spectroscopy is used to investigate the morphology, particle size and element content of the prepared LTO powder. The morphology and distribution of LTO particles size are represented in Fig. 4. The prepared LTO powders are well crystallized and agglomerated. It is noticed that GC1, GC2, GC3 and GC4 with 0.5:1, 1:1, 1.5:2 and 2:1 mass ratio of gelatin and chitosan have average particle sizes of 416 ± 126 nm, 422 ± 77 nm, 391 ± 62 nm and 288 ± 49 nm, respectively. Apparently, the intermolecular interactions of gelatin and chitosan control the aqueous template volume of LTO precursors. When the mass ratio of gelatin to chitosan was 0.5: 1 the template

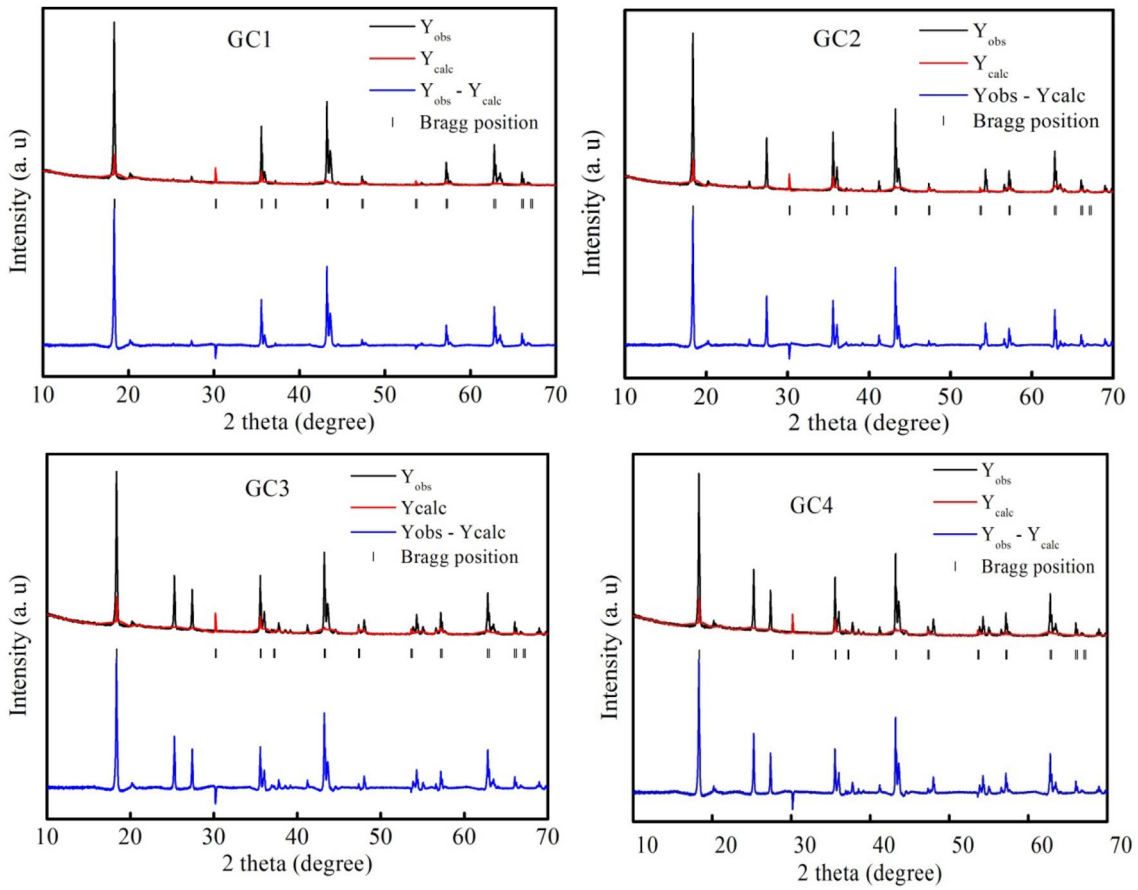


**Fig. 3** Reitveld refined XRD spectrum of the prepared LTO material of **a** GC1 **b** GC2 **c** GC3 **d** GC4 samples

has larger volume. Moreover, the condition of 2: 1 mass ratio of gelatin and chitosan caused smaller volume template due to enhance intermolecular interaction of the polymer active sites. Therefore, the size of LTO powders has been varied from the gelatin and chitosan cross-linked aqueous template. From the morphology it can be seen that increasing the amount of gelatin LTO powders shape changes from plate shape to nearly cubic structural morphology. Thus, gelatin and chitosan finely control the shape and size of the LTO powder.

The element mapping image shown in Fig. 5 prove the presence of Li, Ti and O in the LTO powder. The first element selected in the mapping analysis assumes a red color, the second a green color and third a blue color. In the elemental mapping of GC1, GC2 and GC3, Lithium was selected first followed by Titanium and Oxygen, consequently they have similar color pattern. In GC4 elemental mapping, Titanium was selected before lithium and oxygen and as a result the color pattern changed. All elements show homogeneous distribution. In the diffraction peaks only Ti and O were observed. Fewer amounts of C and Al are present. C presence is due to the combustion of polymer matrices. Al might have present from the sample holder.

FT-IR spectra pattern of the prepared LTO materials are shown in Fig. 6. FT-IR spectrum of the prepared LTO signals at 2360 $cm^{-1}$ and 670 $cm^{-1}$ due to the vibration of Ti–O-Ti and $TiO_6$ octahedron respectively [41, 42]. The absorption bands at 3410 $cm^{-1}$ and 1650 $cm^{-1}$ are characteristic of hydroxyl group [43].

In all the FT-IR spectrum of the LTO samples hydroxyl group peaks detected at two positions. One is around 3400 $cm^{-1}$ and another 1650 $cm^{-1}$. Peaks located at 1490 $cm^{-1}$ and 1090 $cm^{-1}$ are attributed for the anti-symmetric and symmetric stretching vibration of $CO_3^{2-}$ anions, respectively [43]. In the FT-IR spectrum $CO_3^{2-}$ anion and hydroxyl group peaks appeared due to the absorption of $CO_2$ and $H_2O$ on LTO surface [44, 45]. Thus, there is no significant difference of the peak positions in the FT-IR spectrum of all the prepared LTO samples. It implies the presence of a homogeneous Ti–O-Ti bonding pattern in all the prepared LTO samples.

The various functional groups presents in the prepared LTO samples were detected using Raman spectroscopy.

**Table 4** Position of the X-ray peaks, interplanar spacing, corresponding miller indices and calculated lattice constant of the LTO materials

| | | | | | | | | | |
|---|---|---|---|---|---|---|---|---|---|
| GC1 | 2θ | 18.33 | 35.55 | 37.18 | 43.21 | 47.32 | 57.17 | 62.79 | 66.03 |
| | d (Å) | 4.836 | 2.523 | 2.416 | 2.0921 | 1.919 | 1.6093 | 1.4782 | 1.4132 |
| | (hkl) | (111) | (311) | (222) | (400) | (331) | (333) | (440) | (531) |
| | a (Å) | 8.376 | 8.367 | 8.369 | 8.368 | 8.364 | 8.360 | 8.360 | 8.359 |
| | $a_{avg}$ (Å) | 8.365 | | | | | | | |
| | V $(Å)^3$ | 585.32 | | | | | | | |
| | $D_g$ (nm) | 57 | 48 | 149 | 76 | 103 | 113 | 116 | 96 |
| | $D_{g, avg}$(nm) | 94 | | | | | | | |
| GC2 | 2θ | 18.34 | 35.56 | 37.19 | 43.22 | 47.33 | 57.18 | 62.80 | 66.04 |
| | d (Å) | 4.8330 | 2.522 | 2.415 | 2.091 | 1.919 | 1.609 | 1.4784 | 1.413 |
| | (hkl)) | (111) | (311) | (222) | (400) | (331) | (333) | (440) | (531) |
| | a (Å) | 8.371 | 8.364 | 8.365 | 8.364 | 8.364 | 8.360 | 8.360 | 8.359 |
| | $a_{avg}$ (Å) | 8.363 | | | | | | | |
| | V $(Å)^3$ | 584.90 | | | | | | | |
| | $D_g$ (nm) | 57 | 42 | 75 | 76 | 77 | 92 | 95 | 92 |
| | $D_{g, avg}$ (nm) | 75 | | | | | | | |
| GC3 | 2θ | 18.35 | 35.57 | 37.20 | 43.23 | 47.34 | 57.19 | 62.81 | 66.05 |
| | d (Å) | 4.830 | 2.521 | 2.415 | 2.092 | 1.918 | 1.609 | 1.478 | 1.413 |
| | (hkl) | (111) | (311) | (222) | (400) | (331) | (333) | (440) | (531) |
| | a (Å) | 8.365 | 8.361 | 8.365 | 8.368 | 8.360 | 8.360 | 8.360 | 8.359 |
| | $a_{avg}$ (Å) | 8.362 | | | | | | | |
| | V $(Å)^3$ | 584.69 | | | | | | | |
| | $D_g$ (nm) | 47 | 41 | 71 | 43 | 88 | 91 | 74 | 97 |
| | $D_{g, avg}$ (nm) | 69 | | | | | | | |
| GC4 | 2θ | 18.35 | 35.57 | 37.21 | 43.23 | 47.34 | 57.19 | 62.81 | 66.05 |
| | d (Å) | 4.830 | 2.521 | 2.414 | 2.092 | 1.918 | 1.609 | 1.478 | 1.413 |
| | (hkl) | (111) | (311) | (222) | (400) | (331) | (333) | (440) | (531) |
| | a (Å) | 8.365 | 8.361 | 8.362 | 8.368 | 8.360 | 8.360 | 8.360 | 8.359 |
| | $a_{avg}$ (Å) | 8.361 | | | | | | | |
| | V $(Å)^3$ | 584.48 | | | | | | | |
| | $D_g$ (nm) | 47 | 42 | 39 | 39 | 88 | 92 | 73 | 96 |
| | $D_{g, avg}$ (nm) | 64 | | | | | | | |

Figure 7 shows the Raman spectra of the synthesized LTO. This spectrum shows set of peaks appeared at 136, 226, 263, 346, 435, 508, 601 and 660 $cm^{-1}$. Among them five peaks 226, 263, 346, 435 and 660 $cm^{-1}$ highlighted the characteristics of A1g + Eg + 3F2g spinel structure [46–48]. Presence of peak at 226 cm-1 corresponds to the A1g mode and bending vibrations of O-Ti–O bands [49]. The presences of peaks in the range of 500–700 cm-1 are corresponding to Ti–O stretching of $TiO_6$ octahedra of LTO [50, 51]. Apart from them the appearance of peaks in the range 400–550 cm-1 indicate the stretching vibration of Li–O and subsequently confirmed the formation of $LiO_4$ tetrahedral [51]. Thus, such set of Raman bands confirmed the formation of LTO from the calcination of gelatin-chitosan aqua-gel.

Li, O and Ti outermost atomic orbital (2 s), ($2p_x$, $2p_y$, $2p_z$) and (4 s, $3d_{xy}$, $3d_{yz}$, $3d_{zx}$, $3d_{x^2-y^2}$, $3d_{z^2}$) hybridization formed $LiTi_5O_{12}$. These multi orbital hybridization in LTO generated a valence band maximum (O $p_\pi$) and conduction band minimum (Ti $t_{2g}$) gap [52]. Consequently, O and Ti in LTO make major contribution for the direct transition of electron from valence band to conduction band [53]. In this study, UV–visible spectroscopy technique applied to investigate the electronic nature of the prepared LTO materials in ethanol solvent. The characteristics UV–visible absorption spectra of all LTO samples are shown in Fig. 8.

It is noticed that the electron transition peak of all LTO samples appeared after 220 nm, a region of lower wavelengths and higher energies. This may be due to the structural stability of LTO and interaction in presence of a polar solvent ethanol. It is observed that the absorption peak located at 215, 213, 209 and 207 nm for GC1, GC2, GC3 and GC4 samples, respectively. The observed absorption peak variation scales with the content of

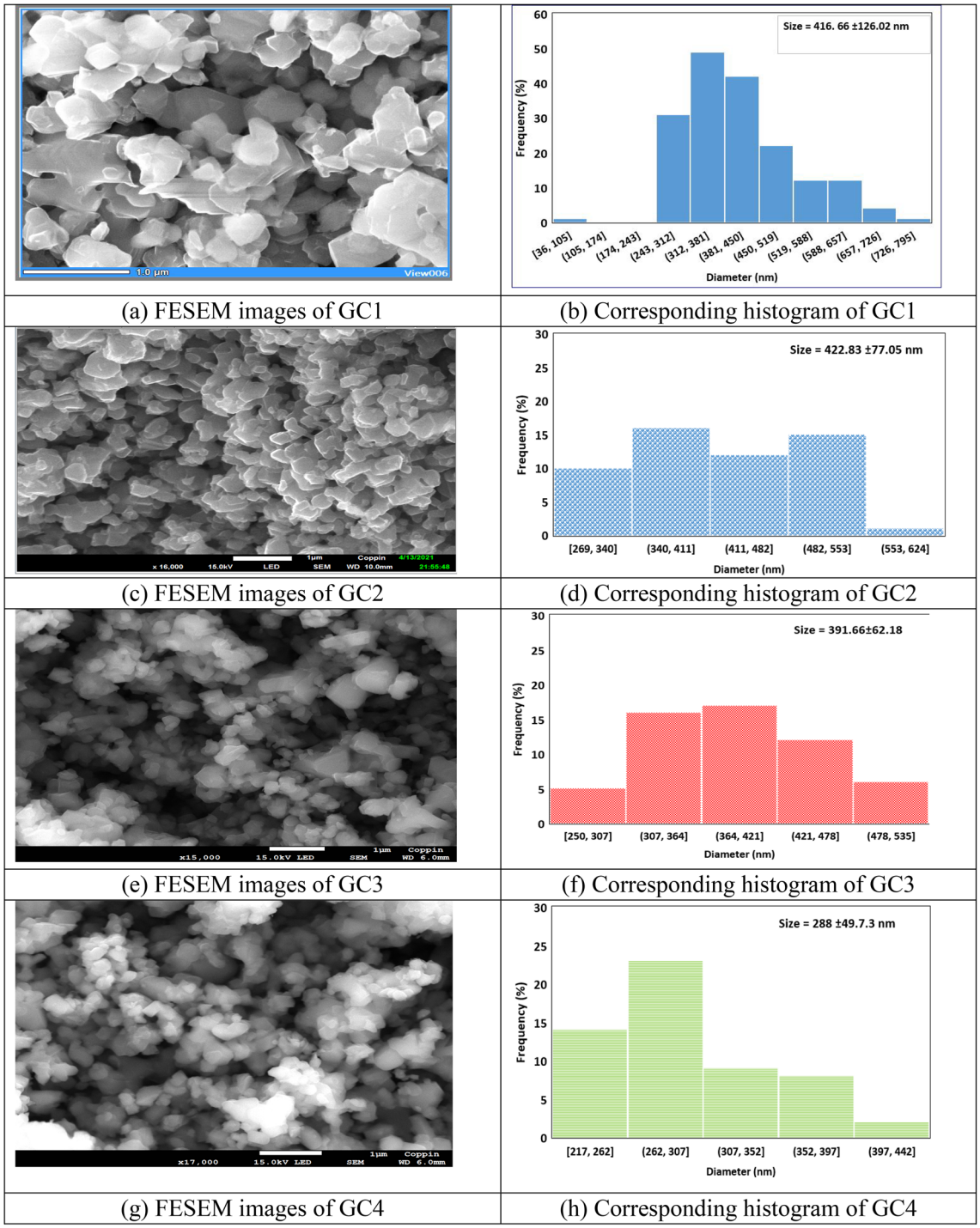


**Fig. 4** FESEM images and corresponding histogram of the prepared LTO powders

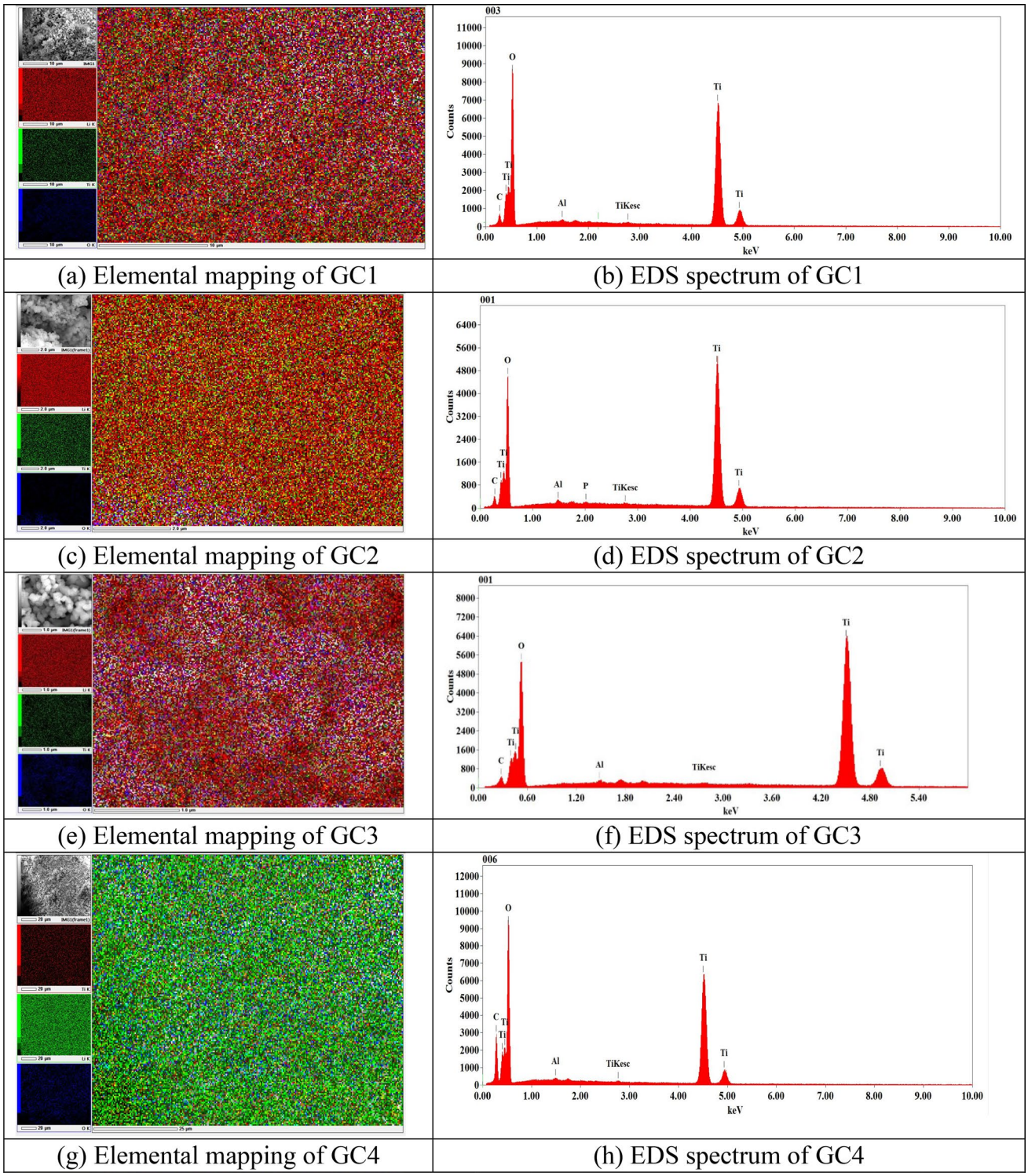


**Fig. 5** Elemental mapping and corresponding EDS spectrum of LTO powders

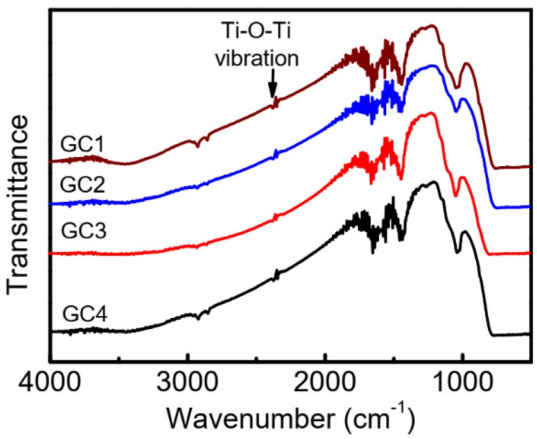


**Fig. 6** FT-IR spectra of the prepared LTO material

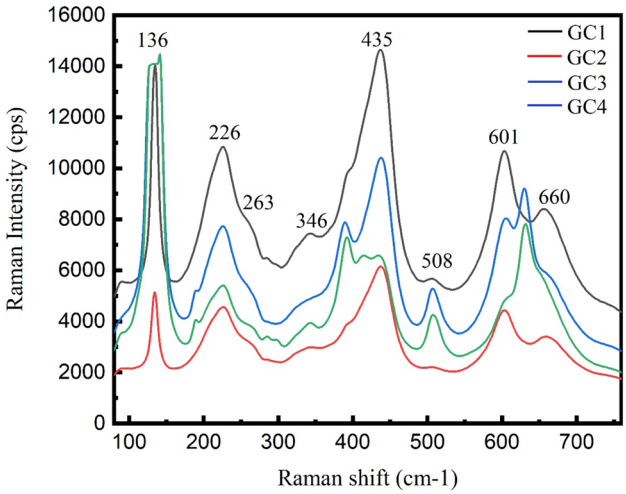


**Fig. 7** Raman spectra of LTO prepared from the calcination of gelatin-chitosan aqua-gel at 750 °C

gelatin in the mass ratio of gelatin to chitosan. The inset of Fig. 8 represents The calculated band gap values are 5.5224, 5.5403, 5.5942 and 5.6071 eV for GC1, GC2, GC3 and GC4 samples, respectively. The efficacy of gelatin and chitosan interaction at various mass ratio prevailed to the optical band gap value. The analyzed UV–visible spectroscopy results are in good agreement with XRD crystallite sizes and FESEM images.

## 4 Conclusion

The present study introduces a versatile pathway of using gelatin and chitosan based aqueous template as an efficient route to tune the morphology and size of LTO powder. The XRD results indicate the formation of highly crystalline LTO material. The appearance of carbon species peaks in the XRD spectrum confirmed the coating of carbon on LTO surface. FESEM observations reveal that LTO particle size reduces by increasing the amount of gelatin at the mass ratio of gelatin to chitosan. Based on the results of UV absorption spectra, it is found that the higher percentage of gelatin in the mass ratio of gelatin to chitosan increases the $E_g$ value of LTO materials. Thus, the study has been proposed a simple and efficient route for tuning the size and morphology of LTO powder.

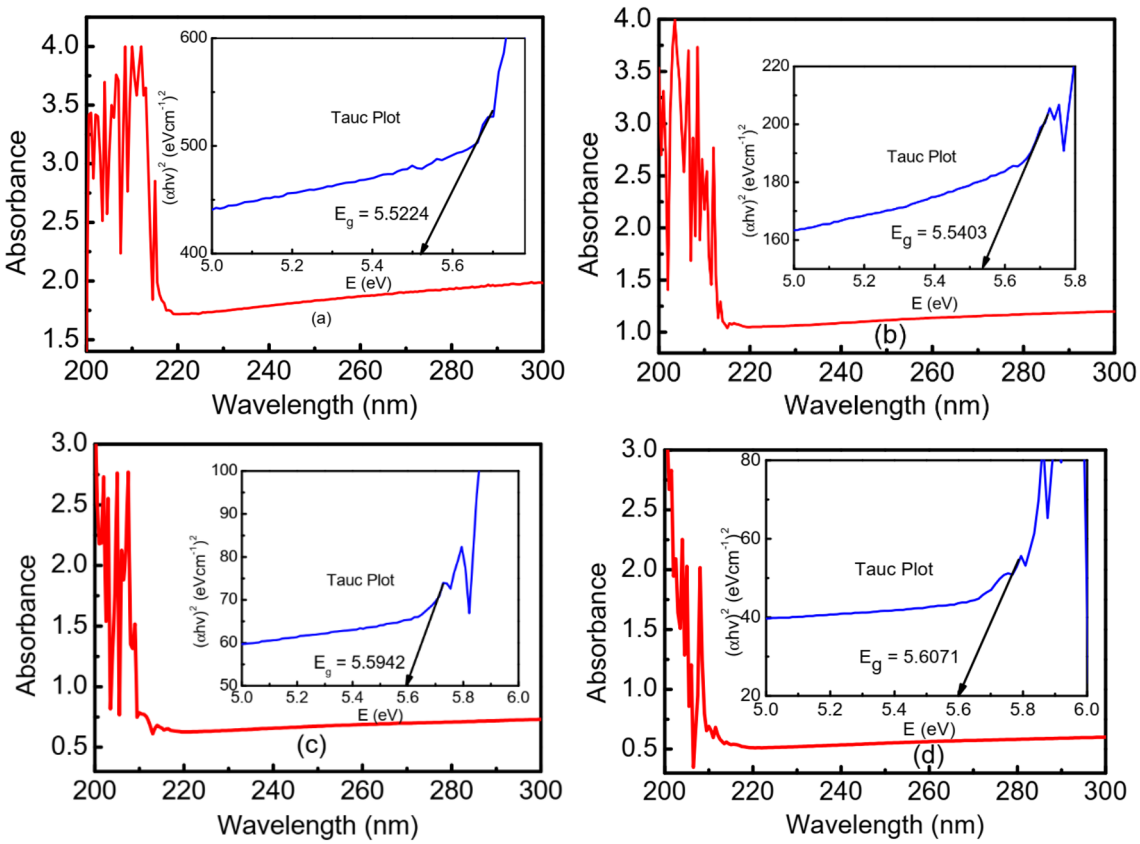


**Fig. 8** UV spectrum of the prepared LTO material of **a** GC1 **b** GC2 **c** GC3 **d** GC4

**Acknowledgements** The Authors gratefully acknowledge the support from the Khulna University of Engineering and Technology, Bangladesh in doing this research.

**Funding** The funding was provided by casr, kuet.

## Declarations

**Conflict of interests** The authors declare that they have no conflict of interests.



## References

1. Li W, Yao L, Zhang X, Lang W, Si J, Yang J, Li L (2020) The effect of chelating agent on synthesis and electrochemical properties of $LiNi_{0.6}Co_{0.2}Mn_{0.2}O_2$. SN Appl Sci 2:1–8
2. Jiao J, Xu Q, Li L (2007) Porous TiO2/SiO2 composite prepared using PEG as template direction reagent with assistance of supercritical CO2. J Colloid Interface Sci 316:596–603
3. Jiang C, Ichihara M, Honma I, Zhou H (2007) Effect of particle dispersion on high rate performance of nano-sized Li4Ti5O12 anode. Electrochim Acta 52:6470–6475
4. Wang QL, Tong DG (2020) Amorphous $LiEuTiO_4$ nano-vesicles as a low-operating potential anode for rechargeable lithium ion batteries. SN Appl Sci 2:1–12
5. Sabarish R, Unnikrishnan G (2019) Synthesis, characterization and evaluations of micro/mesoporous ZSM-5 zeolite using starch as bio template. SN Appl Sci 1:1–13
6. Gurgur E, Oluyamo SS, Adetuyi AO, Omotunde OI, Okoronkwo AE (2020) Green synthesis of zinc oxide nanoparticles and zinc oxide–silver, zinc oxide–copper nanocomposites using Bridelia ferruginea as biotemplate. SN Appl Sci 2:1–12
7. Balakrishnan K, Datar A, Oitker R, Chen H, Zuo J, Zang L (2005) Nanobelt self-assembly from an organic n-type semiconductor: propoxyethyl-PTCDI. J Am Chem Soc 127:10496–10497
8. Love JC, Estroff LA, Kriebel JK, Nuzzo RG, Whitesides GM (2005) Self-assembled monolayers of thiolates on metals as a form of nanotechnology. Chem Rev 105:1103–1170

9. Mann S (2009) Self-assembly and transformation of hybrid nano-objects and nanostructures under equilibrium and non-equilibrium conditions. Nat Mater 8:781–792
10. Zhou Y, Antonietti M (2003) Synthesis of very small $TiO_2$ nanocrystals in a room-temperature ionic liquid and their self-assembly toward mesoporous spherical aggregates. J Am Chem Soc 125:14960–14961
11. Kim S, Alauzun JG, Louvain N, Brun N, Stievano L, Boury B, Monconduit L, Mutin PH (2018) Alginic acid aquagel as a template and carbon source in the synthesis of $Li_4Ti_5O_{12}$/C nanocomposites for application as anodes in Li-ion batteries. RSC Adv 8:32558–32564
12. Ghorbani M, Golobostanfard MR, Abdizadeh H (2017) Flexible freestanding sandwich type ZnO/rGO/ZnO electrode for wearable supercapacitor. Appl Surf Sci 419:277–285
13. Singh N, Salam Z, Subasri A, Sivasankar N, Subramania A (2018) Development of porous $TiO_2$ nanofibers by solvosonication process for high performance quantum dot sensitized solar cell. Sol Energy Mater Sol Cells 179:417–426
14. Pal B, Sharon M (2002) Enhanced photocatalytic activity of highly porous ZnO thin films prepared by sol-gel process. Mater Chem Phys 76:82–87
15. Lv Y, Zhang H, Cao G, Wang B, Wang X (2011) Phenol-formaldehyde resin-assisted synthesis of pure porous $Li_4Ti_5O_{12}$ for rate capability improvement. Mater Res Bull 46:2312–2316
16. Wakayama H, Kawai Y (2019) $LiCoO_2$/$Li_7La_3Zr_2O_{12}$ nanocomposite cathodes synthesized via self-assembled block copolymer templates and used in all-solid-state lithium batteries. Solid State Ionics 334:43–47
17. Liu R, Zhang H, Huang Y, Wang W, Li Z, Yu Z, Wang A, Yuan K (2012) In situ gelatin carbonation to prepare a binder-free $LiFePO_4$ cathode for high-power lithium ion batteries. Electrochim Acta 78:563–568
18. Du H, Yuan C, Huang K, Wang W, Zhang K, Geng B (2017) A novel gelatin-guided mesoporous bowknot-like $Co_3O_4$ anode material for high-performance lithium-ion batteries. J Mater Chem A 5:5342–5350
19. Zhang F, Xu B, Cao G, Chu M, Qiao N, Wei G, Yang Y (2014) Nano/micro structured porous $Li_4Ti_5O_{12}$ synthesized by a polyethylene glycol assisted hydrothermal method for high rate lithium-ion batteries. RSC Adv 4:53981–53986
20. Hong Z, Wei M (2013) Layered titanate nanostructures and their derivatives as negative electrode materials for lithium-ion batteries. J Mater Chem A 1:4403–4414
21. Yuan T, Tan Z, Ma C, Yang J, Ma ZF, Zheng S (2017) Challenges of spinel $Li_4Ti_5O_{12}$ for lithium-ion battery industrial applications. Adv Energy Mater 7:1601625
22. Sun X, Radovanovic PV, Cui B (2015) Advances in spinel $Li_4Ti_5O_{12}$ anode materials for lithium-ion batteries. New J Chem 39:38–63
23. Yi TF, Xie Y, Zhu YR, Zhu RS, Shen H (2013) Structural and thermodynamic stability of $Li_4Ti_5O_{12}$ anode material for lithium-ion battery. J Power Sources 222:448–454
24. Yi TF, Yang SY, Xie Y (2015) Recent advances of $Li_4Ti_5O_{12}$ as a promising next generation anode material for high power lithium-ion batteries. J Mater Chem A 3:5750–5777
25. Aldon L, Kubiak P, Womes M, Jumas JC, Olivier-Fourcade J, Tirado JL, Corredor JI, Pérez Vicente C (2004) Chemical and electrochemical Li-insertion into the $Li_4Ti_5O_{12}$ spinel. Chem Mater 16:5721–5725
26. Zhang SS, Xu K, Jow TR (2006) EIS study on the formation of solid electrolyte interface in Li-ion battery. Electrochim Acta 51:1636–1640
27. Kim JG, Park MS, Hwang SM, Heo YU, Liao T, Sun Z, Park JH, Kim KJ, Jeong G, Kim YJ, Kim JH (2014) $Zr^{4+}$ doping in $Li_4Ti_5O_{12}$ anode for lithium-ion batteries: open $Li^+$ diffusion paths through structural imperfection. Chemsuschem 7:1451–1457
28. Yi TF, Fang ZK, Xie Y, Zhu YR, Yang SY (2014) Rapid charge–discharge property of $Li_4Ti_5O_{12}$–$TiO_2$ nanosheet and nanotube composites as anode material for power lithium-ion batteries. ACS Appl Mater Interfaces 6:20205–20213
29. Han X, Zhao Z, Xu Y, Liu D, Zhang H, Zhao C (2014) Synthesis and characterization of F-doped nanocrystalline $Li_4Ti_5O_{12}$/C compounds for lithium-ion batteries. RSC Adv 4:41968–41975
30. Shen L, Zhang X, Uchaker E, Yuan C, Cao G (2012) $Li_4Ti_5O_{12}$ nanoparticles embedded in a mesoporous carbon matrix as a superior anode material for high rate lithium ion batteries. Adv Energy Mater 2:691–698
31. Kang E, Jung YS, Kim GH, Chun J, Wiesner U, Dillon AC, Kim JK, Lee J (2011) Highly improved rate capability for a lithium-ion battery nano-$Li_4Ti_5O_{12}$ negative electrode via carbon-coated mesoporous uniform pores with a simple self-assembly method. Adv Func Mater 21:4349–4357
32. Li CC, Li QH, Chen LB, Wang TH (2012) A facile titanium glycolate precursor route to mesoporous Au/$Li_4Ti_5O_{12}$ spheres for high-rate lithium-ion batteries. ACS Appl Mater Interfaces 4:1233–1238
33. Zhu JP, Zu W, Zhao JJ, Yang G, Xu QB (2012) Effects of Ag doping and coating on the performance of lithium ion battery material $Li_4Ti_5O_{12}$. J Nanosci Nanotechnol 12:2539–2542
34. Vanin FM, Sobral PJA, Menegalli FC, Carvalho RA, Habitante AMQB (2005) Effects of plasticizers and their concentrations on thermal and functional properties of gelatin-based films. Food Hydrocolloids 19:899–907
35. Baharin A, Haris MRHM, Kartini N, Gunasunderi R, Azura AR (2013) Effect of chitosan loading on mechanical properties, water uptake and toluence absorbency of high and low molecular weight ENR50
36. Cullity BD (1956) Elements of x-ray diffraction. Addison-Wesley Publishing, Boston
37. Tauc J, Menth A (1972) States in the gap. J Non-Cryst Solids 8:569–585
38. Qiao C, Ma X, Zhang J, Yao J (2017) Molecular interactions in gelatin/chitosan composite films. Food Chem 235:45–50
39. Xia Y, Sun B, Wei Y, Tao B, Zhao Y (2017) Simple sol-gel method synthesis of 3-dimension $Li_4Ti_5O_{12}$-$TiO_2$ nanostructures using butterfly wings as biotemplates for high rate performance lithium-ion batteries. J Alloy Compd 705:58–63
40. Wang S, Zhang Y, Abidi N, Cabrales L (2009) Wettability and surface free energy of graphene films. Langmuir 25:11078–11081
41. Li Y, Zhao H, Tian Z, Qiu W, Li X (2008) Solvothermal synthesis and electrochemical characterization of amorphous lithium titanate materials. J Alloy Compd 455:471–474
42. Allen GC, Paul M (1995) Chemical characterization of transition metal spinel-type oxides by infrared spectroscopy. Appl Spectrosc 49:451–458
43. Pasierb P, Komornicki S, Rokita M, Rękas M (2001) Structural properties of $Li_2CO_3$–$BaCO_3$ system derived from IR and Raman spectroscopy. J Mol Struct 596:151–156
44. Zhang DR, Liu HL, Jin RH, Zhang NZ, Liu YX, Kang YS (2007) Synthesis and characterization of nanocrystalline $LiTiO_2$ using a one-step hydrothermal method. J Ind Eng Chem 13:92–96
45. Yan H, Zhu Z, Zhang D, Li W (2012) A new hydrothermal synthesis of spherical $Li_4Ti_5O_{12}$ anode material for lithium-ion secondary batteries. J Power Sources 219:45–51

46. Liu DZ, Hayes W, Kurmoo M, Dalton M, Chen C (1994) Raman scattering of the $Li_{1+x}Ti_{2-x}O_4$ superconducting system. Phys C 235:1203–1204
47. Julien CM, Massot M, Zaghib K (2004) Structural studies of $Li_{4/3}Me_{5/3}O_4$ (Me= Ti, Mn) electrode materials: local structure and electrochemical aspects. J Power Sources 136:72–79
48. Baddour-Hadjean R, Pereira-Ramos JP (2010) Raman microspectrometry applied to the study of electrode materials for lithium batteries. Chem Rev 110:1278–1319
49. Yang LH, Dong C, Guo J (2008) Hybrid microwave synthesis and characterization of the compounds in the Li–Ti–O system. J Power Sources 175:575–580
50. Sandhya CP, John B, Gouri C (2014) Lithium titanate as anode material for lithium-ion cells: a review. Ionics 20:601–620
51. Li X, Lin HC, Cui WJ, Xiao Q, Zhao JB (2014) Fast solution-combustion synthesis of nitrogen-modified $Li_4Ti_5O_{12}$ nanomaterials with improved electrochemical performance. ACS Appl Mater Interfaces 6:7895–7901
52. Gould T, Su Z, Zhang S (2019) Why electrochromism in $Li_4Ti_5O_{12}$ differs in the visible and infrared spectrum
53. Nguyen TDH, Pham HD, Lin SY, Lin MF (2019) Enrich properties of $Li^+$-based battery anode: $Li_4Ti_5O_{12}$